

# Journal of Materials Chemistry A

Accepted Manuscript



This is an *Accepted Manuscript*, which has been through the Royal Society of Chemistry peer review process and has been accepted for publication.

*Accepted Manuscripts* are published online shortly after acceptance, before technical editing, formatting and proof reading. Using this free service, authors can make their results available to the community, in citable form, before we publish the edited article. We will replace this *Accepted Manuscript* with the edited and formatted *Advance Article* as soon as it is available.

You can find more information about *Accepted Manuscripts* in the [Information for Authors](#).

Please note that technical editing may introduce minor changes to the text and/or graphics, which may alter content. The journal's standard [Terms & Conditions](#) and the [Ethical guidelines](#) still apply. In no event shall the Royal Society of Chemistry be held responsible for any errors or omissions in this *Accepted Manuscript* or any consequences arising from the use of any information it contains.



## Efficient Hole Transport Layers with Widely Tunable Work Function for Deep HOMO Level Organic Solar Cells

Jiaqi Cheng<sup>#a</sup>, Fengxian Xie<sup>#a</sup>, Yongsheng Liu<sup>b</sup>, Wei E.I. Sha<sup>a</sup>, Xinchen Li<sup>a</sup>, Yang Yang<sup>\*b</sup>, Wallace C.H. Choy<sup>\*a</sup>

Received 00th January 20xx,  
Accepted 00th January 20xx

DOI: 10.1039/x0xx00000x

www.rsc.org/

Hole transport layers (HTLs) with large work function (WF) tuning ability for good energy level alignment with deep highest occupied molecular orbital (HOMO) level donor materials are desirable for high-performance and high open-circuit voltage ( $V_{oc}$ ) organic solar cells (OSCs). Here, a novel low-temperature and solution-process approach to achieve WF tuning in HTLs is proposed. Specifically, the HTLs made from 2,3,4,5,6-pentafluorobenzylphosphonic acid (F5BnPA) incorporated graphene oxide (GO) and molybdenum oxide ( $\text{MoO}_x$ ) solution (representing two possible classes of HTLs where carriers transport via valence and conduction bands, respectively) offer continuous WF tuning (the tuning range as large as 0.81 eV) by controlling F5BnPA's concentration. By employing a deep HOMO donor material, OSCs using the composite HTLs can achieve improved performances with largely increased  $V_{oc}$  (0.92 V for GO:F5BnPA versus 0.65 V for pristine GO; 0.91 V for  $\text{MoO}_x$ :F5BnPA versus 0.88 V for pristine  $\text{MoO}_x$ ). The enhanced performance can be experimentally and theoretically explained by the decreased hole injection barrier (HIB) for GO or equivalent HIB (i.e. electron extraction barrier) for  $\text{MoO}_x$  and enhanced surface recombination velocity, which contribute to eliminating S-shaped current-voltage characteristics. Consequently, the incorporation of F5BnPA can efficiently tune HTL WF for high  $V_{oc}$  OSCs and extend HTL applications in organic electronics.

### Introduction

As an attractive low-cost alternative to traditional photovoltaics technologies, organic solar cells (OSCs) have been experiencing a remarkable leap in power conversion efficiency (PCE) approaching over 10% both in single junction OSCs and in tandem OSCs during the past decade.<sup>1-6</sup> These substantial research advances benefit enormously from the engineering of material synthesis (novel organic photoactive polymers/small molecules),<sup>7-9</sup> film morphology,<sup>10</sup> device structure (normal/inverted and tandem structures),<sup>11, 12</sup> interfacial carrier-transport layers<sup>13-15</sup> and the understanding of device physics<sup>16, 17</sup>. Among these aspects, the interface between electrodes and active layers plays an important role in determining the performance of OSCs. Mismatched Fermi level of electrodes with the corresponding Fermi levels for holes and electrons of organic active layers will result into the formation of extraction/injection barriers at the interface, impairing the electrical property and thus the device performance of OSCs.<sup>18, 19</sup> Charge carriers selective contacts

that extract holes (electrons) only and block the injection of counter electrons (holes) from organic active layers will reduce the loss of photogenerated charge carriers and raise open-circuit voltage ( $V_{oc}$ ).<sup>20-23</sup> Therefore, the design of functional carrier-transport layers between electrodes and organic active layers is highly important and desirable for high-performance OSCs.

Regarding hole transport layers (HTLs), poly(3,4-ethylenedioxythiophene):poly(styrene-sulfonate) (PEDOT:PSS) is commonly used as the HTL in fabricating standard OSCs. However, its long-term acidity and hygroscopic nature will induce poor stability of OSCs and then severely degrade devices.<sup>24</sup> Alternatively, various oxides have been developed as substitutes of PEDOT:PSS for high performance and stable OSCs. These oxides can be classified as two types according to their carrier transport mechanisms. Molybdenum oxide ( $\text{MoO}_x$ ),<sup>25-27</sup> vanadium oxide ( $\text{V}_2\text{O}_5$ ),<sup>25, 28</sup> tungsten oxide ( $\text{WO}_3$ ),<sup>25, 29</sup> and etc. have very large ionization potential (IP), which precluded hole transport via valence band (VB). The hole extraction can be processed via the electron transport from the electrode through the oxides conduction band (CB) to the highest occupied molecular orbital (HOMO) of organic donors.<sup>25</sup> Differently, for another class of oxides including graphene oxide (GO),<sup>30-32</sup> nickel oxide ( $\text{NiO}_x$ ),<sup>14, 33, 34</sup> and etc., hole transport via VB of the metal oxide is favorable. The WF of these HTL materials (PEDOT:PSS 5.1 eV, GO 4.9 eV,  $\text{NiO}_x$  5.4 eV,  $\text{MoO}_x$  5.3 eV,  $\text{V}_2\text{O}_5$  5.4 eV,  $\text{WO}_3$  5.35 eV) can align well with

<sup>#</sup>These authors contributed equally to this work.

<sup>a</sup>Department of Electrical and Electronic Engineering, The University of Hong Kong, Pokfulam Road, Hong Kong SAR, China. Email: chchoy@eee.hku.hk

<sup>b</sup>Department of Materials Science and Engineering, University of California, Los Angeles, Los Angeles, CA 90095, USA. Email: yangy@ucla.edu

<sup>†</sup>Electronic Supplementary Information (ESI) available: [details of any supplementary information available should be included here]. See DOI: 10.1039/x0xx00000x

HOMO levels of many typical organic photoactive donors such as poly(3-hexylthiophene) (P3HT) (5.1 eV), polythieno[3,4-b]-thiophene-co-benzodithiophene (PTB7) (5.14 eV).<sup>35</sup> Importantly, high  $V_{OC}$  values contribute to the realization of high-performance OSCs. Since maximum value of the  $V_{OC}$  is determined by the energy offset between the HOMO level of the donor and the lowest occupied molecular orbital (LUMO) level of the acceptor, conjugated polymer/small molecule donor materials with deep HOMO levels (typically > 5.5 eV) is attractive for obtaining high  $V_{OC}$  values. To avoid the formation of hole injection barrier (HIB) at the interface, designing suitable HTL materials for these polymers/small molecule donor materials with deep HOMO levels is highly desirable.

The design of ideal HTL materials for these deep HOMO-level polymers/small molecules, combining the requirements of smooth surface, good tuning ability of indium-tin oxide (ITO) WF and good electron blocking ability with efficient hole transport, remains challenging. Several WF tuning methods of GO have been reported, including  $O_2$  plasma treatment,<sup>36</sup> sulfuration,<sup>37</sup> chlorination,<sup>32</sup> photo chlorination<sup>38</sup> and pre-oxidation.<sup>39</sup> Besides, WF tuning methods of GO for electron transporting layer (ETL) application has also been reported, including cesium neutralization<sup>40</sup> and lithium-neutralization.<sup>41</sup> More details can be found from the review article by Liu et al.<sup>42</sup> However, all the reported WF tuning methods for HTL application need energy-wasting and complex chemical reaction process. Moreover, the reported WF can only be modified to as high as ~5.2 eV, which is still not high enough to match with deep HOMO level (> 5.5 eV) donors. Solution-process phosphonic acid has been reported to be a good surface modifier of oxide layer such as ITO,<sup>43, 44</sup> zinc oxide (ZnO)<sup>45-47</sup> and  $NiO_x$ .<sup>48</sup> These modification effects are ascribed to the chemisorption between the phosphate group and the oxide layer surface, including covalent bonding, electrostatic interactions and hydrogen bonding.<sup>49</sup> While phosphonic acid modified ITO has been reported in OSCs using deep HOMO level donors, such as poly(N-9'-heptadecanyl-2,7-carbazole-alt-5,5-(4',7'-di-2-thienyl-2',1',3'-benzothiadiazole) (PCDTBT) and poly(p-phenylenevinylene) derivative (Super Yellow, SY) with improved  $V_{OC}$ , the surface modification process is accompanied with complicated procedures such as long soaking process for 24 hours, complex rinse and dry procedures, as well as even high temperature annealing.<sup>48, 50-54</sup> Consequently, it is of strong importance to develop a simple low-temperature and solution-process approach for designing effective HTL materials combining smooth surface, good ability of WF tuning and good electron blocking ability with efficient hole transport ability.

In this work, we demonstrate a facile low-temperature and solution-process method to design efficient phosphonic acid modified HTL materials (GO and  $MoO_x$ ) with wide WF tuning capabilities for deep HOMO-level polymer/small molecule donors. By adding controllable amount of 2,3,4,5,6-pentafluorobenzylphosphonic acid (F5BnPA) (as shown in ESI Fig. S1a) into individual GO and  $MoO_x$  solutions, we can realize

a tunable WF (the value can be as high as 5.78 eV) of resultant HTLs made from the two individual oxides on ITO substrates.† Employing a deep HOMO-level two-dimensional conjugated small molecule (SMPV1) donor, OSCs using the composite HTLs can achieve improved performance, especially with increased  $V_{OC}$  (0.65 V for pristine GO versus 0.92 V for GO:F5BnPA; 0.88 V for pristine  $MoO_x$  versus 0.91 V for  $MoO_x$ :F5BnPA). These performance improvement indicates the wide feasibility in the two classes of HTL materials (carrier transport via CB and VB respectively). The experimental and theoretical evidence show that the enhanced performance in F5BnPA-modified OSCs can be explained by the decreased HIB and enhanced surface recombination velocity. This new approach can offer an effective mean for tuning the WF of HTLs to be well aligned with deep HOMO-level polymer/small molecule donor materials, which provides a simple scheme to fabricate high  $V_{OC}$  and high-performance OSCs.

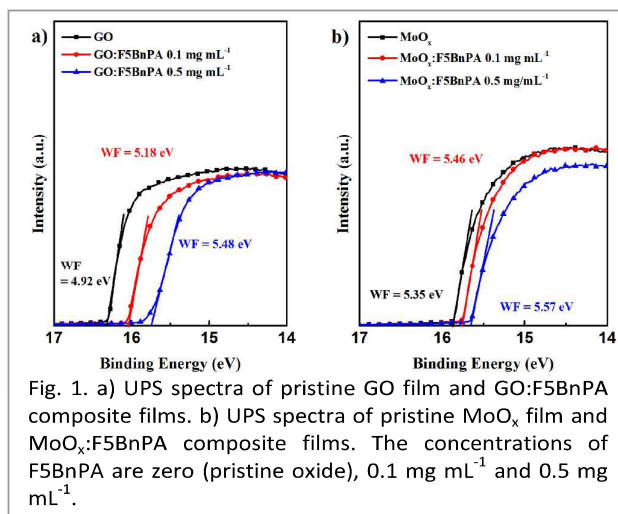
## Results and Discussion

### Continuously and Wide Tuning the WF of HTL Materials

For the current work, we incorporate different amount of F5BnPA into GO and  $MoO_x$  solutions for forming HTL with continuous and controllable tuning of WF. Details of the oxide solution and films preparation have been described in Experimental Section. Solutions of GO:F5BnPA and  $MoO_x$ :F5BnPA with different concentrations of F5BnPA are prepared by simply adding different amounts of F5BnPA into GO and  $MoO_x$  solutions, respectively. Kelvin-Probe measurement is employed to investigate the WF variation through incorporating different concentration of F5BnPA, as shown in Table 1. The pristine GO film on ITO substrates exhibits a WF of 4.91 eV, which does not match well with deep HOMO-level polymer/small molecule donor materials (typically > 5.5 eV). After adding different concentrations of F5BnPA, the WF of the composite film can be tuned continuously from 4.91 eV to 5.72 eV (i.e. WF variation of 0.81 eV). Similarly, the WF of  $MoO_x$ :F5BnPA can be adjusted from 5.30 eV (pristine  $MoO_x$ ) to 5.78 eV at the additive concentration of 1 mg mL<sup>-1</sup>. The WF tuning variations for GO:F5BnPA and  $MoO_x$ :F5BnPA HTLs

Table 1. The WF of GO and  $MoO_x$  films with different concentrations of F5BnPA characterized by Kelvin-Probe measurement.  $\Delta E_F$  is defined as the energy level offsets of the composite film and pristine films. The WF of ITO is listed for comparison.

Concentrations of F5BnPA (mg mL <sup>-1</sup> )	GO:F5BnPA		$MoO_x$ :F5BnPA	
	$W_F$ (eV)	$\Delta E_F$ (eV)	$W_F$ (eV)	$\Delta E_F$ (eV)
ITO			4.69	
w/o	4.91	0	5.30	0
0.1	5.13	0.22	5.48	0.18
0.25	5.43	0.52	5.52	0.22
0.5	5.52	0.61	5.58	0.28
0.75	5.65	0.74	5.67	0.37
1	5.72	0.81	5.78	0.48

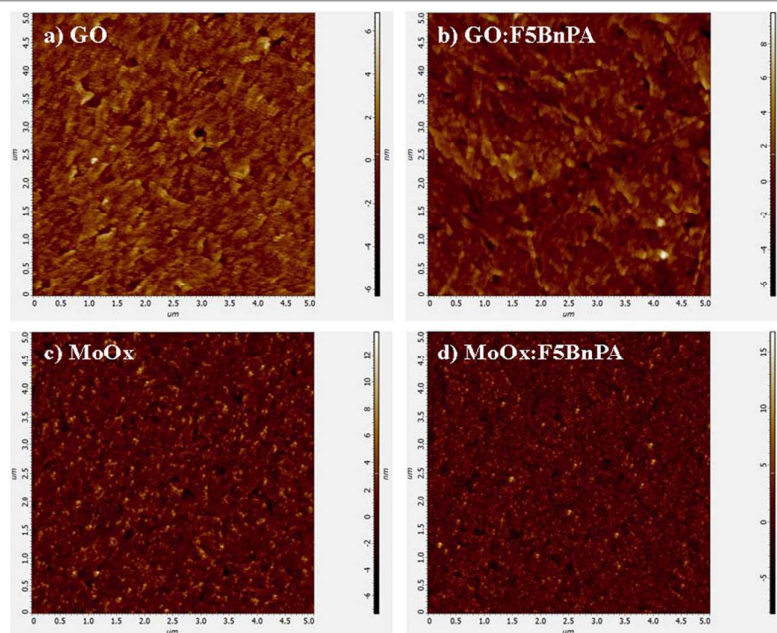


measured by Kelvin-Probe are 0.81 eV and 0.48 eV, respectively.

To further clarify the capability of WF tuning by F5BnPA additive in oxide HTL materials, these films are characterized by ultraviolet photoelectron spectra (UPS) and Kelvin-Probe force microscope (KPFM), as shown in Fig. 1 and Fig. S2. It can be seen from Fig. 1a that the pristine GO films show a WF of 4.92 eV that is consistent with other reports.<sup>30</sup> After adding two different amounts of F5BnPA, 0.1 mg mL<sup>-1</sup> and 0.5 mg mL<sup>-1</sup>, the corresponding resultant films show increased WF of 5.18 eV and 5.48 eV, respectively. Similarly, Fig. 1b shows that the results of MoO<sub>x</sub> film in which WF is 5.35 eV (pristine MoO<sub>x</sub>), 5.46 eV (0.1 mg mL<sup>-1</sup> of F5BnPA) and 5.57 eV (0.5 mg mL<sup>-1</sup> of F5BnPA). Evidently, the UPS spectra further confirm this continuously tuning WF of F5BnPA-modified GO and MoO<sub>x</sub>

composite films, which is consistent with the results obtained by Kelvin-Probe measurement. Fig. S2 shows the KPFM images of GO, GO:F5BnPA, MoO<sub>x</sub> and MoO<sub>x</sub>:F5BnPA. The concentration of F5BnPA is 0.1 mg mL<sup>-1</sup>. The smooth surface potential reveals that good film quality is formed after the F5BnPA incorporation. And the more negative surface potential values after incorporation certify the WF increase as demonstrated by Kelvin-Probe characterization and UPS.<sup>55</sup>

This WF tuning might be ascribed to the chemisorption between F5BnPA and the oxide surface. As we all know, GO is a graphene sheet functionalized with epoxy and hydroxyl groups on its sheet panel and at the edges.<sup>36</sup> Heterocondensation and covalent bond formation will happen between phosphonate groups and hydroxyl groups.<sup>49</sup> Due to highly electronegative fluorine atoms on the aromatic ring of F5BnPA, a surface dipole pointing away from the surface forms on the surface, which results in the increase of WF as shown in ESI Fig. S3.† MoO<sub>x</sub> is a layered crystal structure held by van der Waals forces with hydroxyl groups on the surface.<sup>28,56</sup> F5BnPA is also easily bound to metal oxide surfaces, which also results in a surface dipole and WF increase. Besides, the Lewis acidic property of MoO<sub>x</sub> helps with the chemisorption.<sup>57</sup> Moreover, it is indicated that the WF change of GO is approximately twice the one for MoO<sub>x</sub>. This phenomenon could be ascribed to the different thickness of GO and MoO<sub>x</sub>. As the optimized thickness of GO and MoO<sub>x</sub> for OSCs application is 2 nm and 8 nm respectively (see the following section) and only the surface dipole contributes to the WF change, GO gets larger WF change after blending with the same amount of F5BnPA. The broad tuning WF of F5BnPA-modified GO and MoO<sub>x</sub> films enables the HTLs to match with deep HOMO-level donors in OSCs, such as 1,1-bis-(4-bis(4-methyl-phenyl)-amino-phenyl)-



## ARTICLE

## Journal of Materials Chemistry A

cyclohexane (TAPC, 5.5 eV),<sup>58</sup> PCDTBT, 5.5 eV,<sup>59</sup> poly[N-9'-heptadecanyl-2,7-carbazole-alt-5,5-(4,7-di-2-thienyl-5,6-bis(dodecyloxy)-2,1,3-benzothia-diazole)] PCDTBT12, 5.6 eV),<sup>60</sup> and to be used in other organic devices such as organic light emitting diodes.

The morphology of GO, GO:F5BnPA, MoO<sub>x</sub> and MoO<sub>x</sub>:F5BnPA films have also been investigated by atomic force microscope (AFM) as shown in Fig. 2. The concentration of F5BnPA is 0.5 mg mL<sup>-1</sup> for both GO and MoO<sub>x</sub>. The root-mean-square (RMS) roughness of GO, GO:F5BnPA, MoO<sub>x</sub> and MoO<sub>x</sub>:F5BnPA are measured to be 1.11 nm, 1.37 nm, 1.93 nm and 2.22 nm, respectively. The small RMS indicates that GO and MoO<sub>x</sub> can form compact and smooth buffer layer on ITO substrates and the addition of F5BnPA has little influence on the roughness.

### Performance of Organic Solar Cells

To study the impact of F5BnPA-incorporated GO and MoO<sub>x</sub> HTL films on device performance, a two-dimensional conjugated small molecule (SMPV1) with a deep HOMO level (5.51 eV)<sup>1</sup> is used as the donor material. [6,6]-phenyl C<sub>71</sub>-butyric acid methyl ester (PC<sub>71</sub>BM) is employed as the acceptor material. Their corresponding chemical structures are shown in ESI Fig. S1b.† OSCs with the structure of ITO/HTLs/SMPV1:PC<sub>71</sub>BM/Ca/Al are fabricated, as detailed in Experimental Section. The optimized film thickness of GO and MoO<sub>x</sub> are 2 nm and 8 nm respectively as measured by an ellipsometer. The device performance of OSCs with different thickness of GO and MoO<sub>x</sub> are shown in ESI Fig. S4.†

The typical current density-voltage (*J-V*) curves under an AM 1.5G illumination are shown in Fig. 3 and the performance of optimized OSCs are summarized in Table 2. By incorporating F5BnPA to form the GO:F5BnPA HTL (the concentration of F5BnPA is 0.5 mg mL<sup>-1</sup>), the optimized OSCs achieve increased short-circuit current density (*J<sub>sc</sub>*) of 11.96 mA cm<sup>-2</sup> (11.03 mA cm<sup>-2</sup> for pristine GO OSC), largely increased *V<sub>oc</sub>* of 0.92 V (0.65 V), fill factor (FF) of 46.59% (43.28%), and PCE of 5.13% (3.10%). Similarly, by replacing MoO<sub>x</sub> HTL with MoO<sub>x</sub>:F5BnPA HTL (the concentration of F5BnPA is 0.5 mg mL<sup>-1</sup>), optimized devices display gradually enhanced *J<sub>sc</sub>* of 11.69 mA cm<sup>-2</sup> (10.96 mA cm<sup>-2</sup> for pristine MoO<sub>x</sub> OSCs), moderately enhanced *V<sub>oc</sub>* of 0.91 V (0.88 V), FF of 55.92% (50.81%), and PCE of 5.96% (4.92%), which is comparable with PEDOT:PSS based devices as shown in Fig. S5 and Table S1.† The external quantum efficiency (EQE) spectra of these OSCs are illustrated in ESI Fig. S6.† Compared with OSCs using pristine GO or MoO<sub>x</sub> HTLs, OSCs using the F5BnPA incorporated HTLs achieve higher EQE. Moreover, S-shaped deformation of *J-V* characteristics is also

observed in OSCs using pristine GO or MoO<sub>x</sub> HTLs (Fig. 3b and c). After incorporating F5BnPA, these S-shaped *J-V* characteristics are eliminated. The underlying physics will be discussed below in details experimentally and theoretically.

The performance improvement and the elimination of S-shape *J-V* curve can be analyzed through the schematic energy level diagram as shown in Fig. 3a. When pristine GO film is used as the HTL, there is a large energy level offset (ca. 0.6 eV) at ITO/active layer interface. The energy level offset is ca. 0.15 eV when pristine MoO<sub>x</sub> is used at the HTL. Typically, *V<sub>oc</sub>* is determined by the built-in potential in OSCs.<sup>61</sup> For unoptimized interface contact, the WF of electrodes will limit the *V<sub>oc</sub>*. Thus, the larger energy level offset in GO based devices results in the bigger *V<sub>oc</sub>* suppression (0.27 V) compared with 0.03 V in MoO<sub>x</sub> based devices. Furthermore, the large energy level offset can lead to the formation of hole injection barriers for GO (or equivalent hole injection barrier, i.e. electron extraction barrier for MoO<sub>x</sub>), which has been reported to be responsible for the S-shaped *J-V* characteristics.<sup>23,62</sup> By introducing F5BnPA, the WF of HTLs is in good alignment with the HOMO level of donors, thus the interfacial energy loss will be minimized and *V<sub>oc</sub>* can be increased. The decreased (equivalent) HIB also contributes to the suppression of S-shaped *J-V* curves. In addition, the dark current rectification ratio of approximately 300 for pristine GO based OSCs at ± 2 V is achieved as shown in Fig. 3d, which greatly increases to ca. 7500 for GO:F5BnPA based OSCs. For MoO<sub>x</sub> case, the rectification ratio increases from 1.0×10<sup>5</sup> (pristine MoO<sub>x</sub>) to 3.5×10<sup>5</sup> for MoO<sub>x</sub>:F5BnPA based OSCs, as shown in Fig. 3e. The largely increased rectification ratio for both cases indicates that GO/MoO<sub>x</sub>:F5BnPA HTLs offer better alignment between ITO substrates and HOMO-level of donors, and thus provide a better hole injection contact.

To further illustrate the improvement of hole transporting properties, hole only devices with the structure of ITO/HTL/SMPV1:PC<sub>71</sub>BM/MoO<sub>x</sub>/Ag were fabricated. A comparison of the *J-V* characteristics are as shown in Fig. S7.† The hole transportation gets enhanced after the incorporation of F5BnPA. Hole mobilities were derived by fitting the *J-V* curves in the square law region according to space charge limit current (SCLC) model and the Mott-Gurney law,<sup>63</sup>

$$J = (9/8)\epsilon_r\epsilon_0\mu(V^2/L^3)$$

where *J* is the current density,  $\epsilon_r$  is the relative permittivity,  $\epsilon_0$  is the permittivity of free space,  $\mu$  is the hole mobility, *V* is the applied voltage, *L* is the thickness of active layer. Hole mobilities of 3.04 × 10<sup>-5</sup>, 6.76 × 10<sup>-5</sup>, 5.77 × 10<sup>-5</sup> and 1.07 × 10<sup>-4</sup> cm<sup>2</sup> V<sup>-1</sup> s<sup>-1</sup> have been determined for the devices with GO,

Table 2. Device performance of OSCs with the structure of ITO/HTL/SMPV1:PC<sub>71</sub>BM/Ca/Al.

	<i>J<sub>sc</sub></i> (mA cm <sup>-2</sup> )	<i>V<sub>oc</sub></i> (V)	FF (%)	PCE (%)
GO	11.03 ± 0.27	0.65 ± 0.01	43.28 ± 0.76	3.10 ± 0.14
GO:F5BnPA	11.96 ± 0.11	0.92 ± 0.01	46.59 ± 1.00	5.13 ± 0.18
MoO <sub>x</sub>	10.96 ± 0.20	0.88 ± 0.01	50.81 ± 0.30	4.92 ± 0.10
MoO <sub>x</sub> :F5BnPA	11.69 ± 0.27	0.91 ± 0.01	55.92 ± 0.90	5.96 ± 0.19

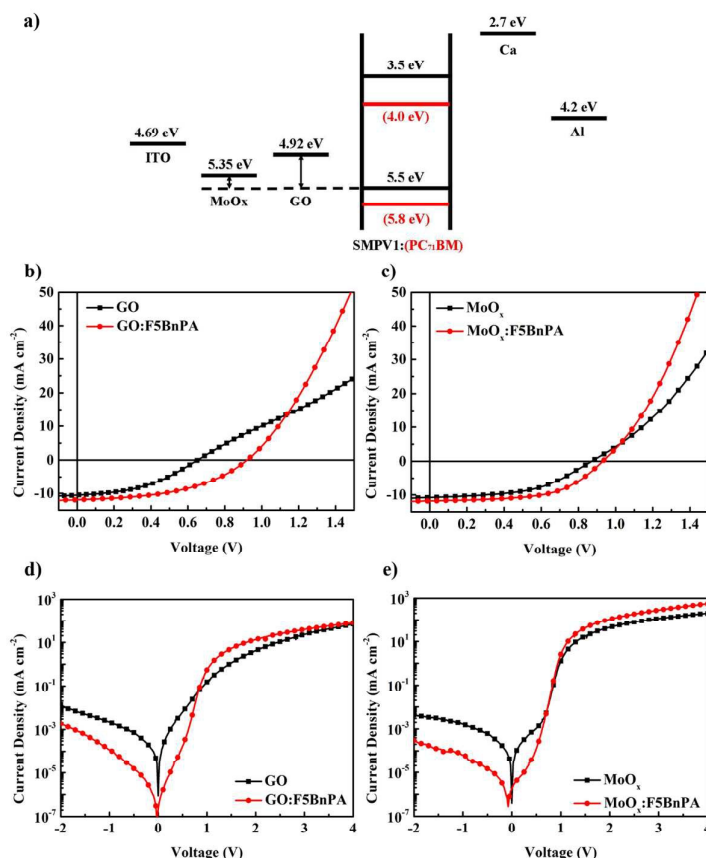


Fig. 3. a) The schematic energy level diagram of OSCs. b, c) Current density-voltage ( $J$ - $V$ ) characteristics of OSCs using different HTLs (the concentrations of F5BnPA are both  $0.5 \text{ mg mL}^{-1}$ ) under illumination of simulated  $100 \text{ mW cm}^{-2}$  AM 1.5G irradiation. d, e) Corresponding dark  $J$ - $V$  curves measured.

GO:F5BnPA, MoO<sub>x</sub>, MoO<sub>x</sub>:F5BnPA as HTLs. The improved hole mobility after incorporation of F5BnPA indicates better hole transport in OSCs.

Fig. 4 shows the light intensity dependent  $V_{OC}$  for OSCs with and without the addition of F5BnPA. We can see a linear increase of  $V_{OC}$  by the logarithm scale of light intensity. The slopes for the devices based on GO and MoO<sub>x</sub> HTLs are 0.64 and 0.81, which increase to 0.96 and 0.95 after separately introducing F5BnPA additives, indicating bimolecular recombination dominated recombination dynamics<sup>64-66</sup> in GO:F5BnPA and MoO<sub>x</sub>:F5BnPA based OSCs. The changes of the slopes through the incorporation of different concentrations of F5BnPA observed as shown in Fig. 4 strongly depend on the (equivalent) hole injection barriers and surface recombination velocity as discussed in details theoretically in the following section. The experimental and theoretical (as will be discussed later) studies show that the incorporation of F5BnPA in HTLs can reduce the HIB and enhance the surface recombination velocity.

#### Theoretical Investigation on F5BnPA Induced Performance Improvement

The electrical contact, which controls collections of photogenerated carriers (electrons and holes), is highly important to electrical properties of OSCs. An ideal contact should satisfy two essential requirements: (1) a zero injection barrier; (2) an infinite surface recombination velocity. A large injection barrier or finite surface recombination velocity will block and accumulate charges at electrodes and thus modify the built-in electrostatic field, which significantly degrade the electrical performance of OSCs. Meanwhile, to our best

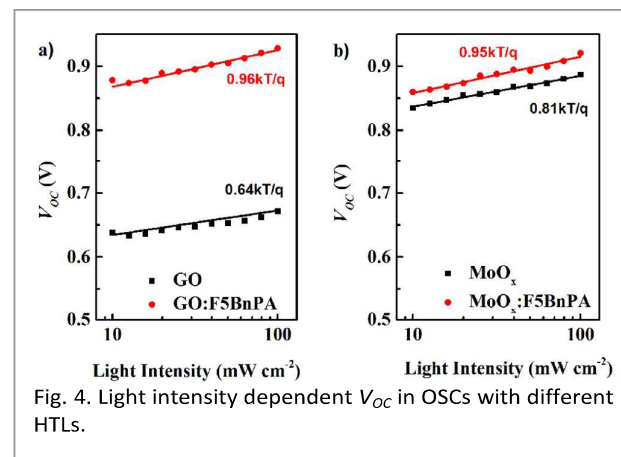


Fig. 4. Light intensity dependent  $V_{OC}$  in OSCs with different HTLs.

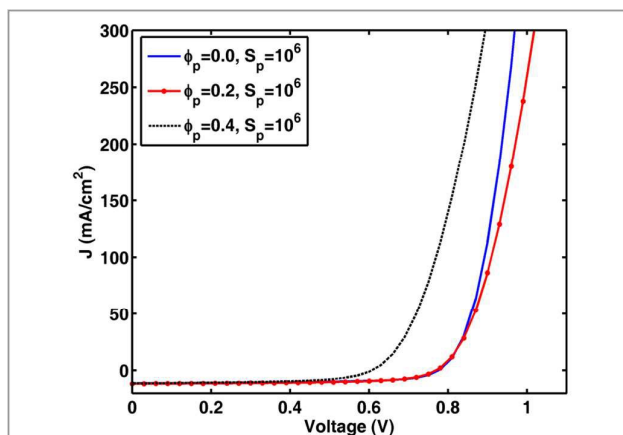


Fig. 5. Simulated  $J$ - $V$  characteristics of OSCs with different injection barriers between anode and active layer. An approximately infinite surface recombination velocity for holes at the anode (with a value of  $S_p = 10^6 \text{ m s}^{-1}$ ) is assumed.  $\phi_p$  is the injection barrier at the anode with the unit of eV.

knowledge, few theoretical works systemically investigated the evolution of the relation between  $V_{OC}$  and incident light intensity ( $I$ ) as the electrode interface is modified. This investigation is highly important to electrode-related device physics and thus high-efficient solar cells.

To investigate the influence of different anode configurations (GO,  $\text{MoO}_x$ , GO:F5BnPA and  $\text{MoO}_x$ :F5BnPA) on electrical properties of OSCs, semiconductor equations (Poisson, drift-diffusion, and continuity equations) are solved self-consistently (see Theoretical Model in Experimental Section). The cathode can be regarded as a good ohmic contact by using Ca/Al electrode. Fig. 5 shows the simulated  $J$ - $V$  characteristics of OSCs with different injection barriers at the anode-active layer interface. When the (equivalent) injection barrier is formed at the interface,  $J$ - $V$  curve at the forward bias regime will bend toward high-voltage direction and meanwhile  $V_{OC}$  is reduced. These features agree well with the experimental

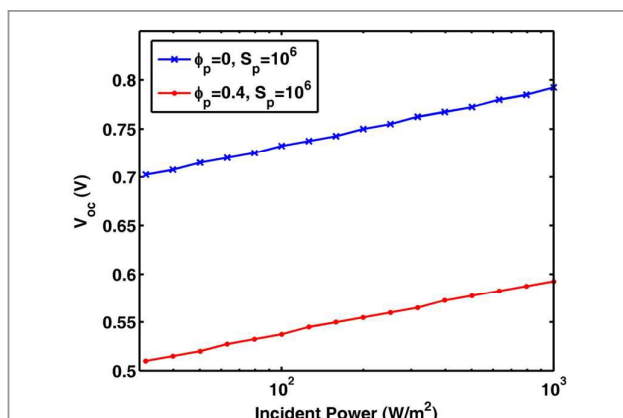


Fig. 6. Simulated  $V_{OC}$  versus incident light intensity with different injection barriers between anode and active layer. An approximately infinite surface recombination velocity for holes at the anode (with a value of  $S_p = 10^6 \text{ m s}^{-1}$ ) is assumed.

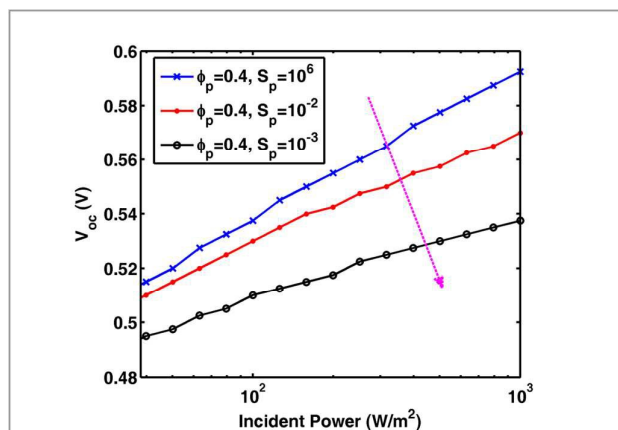


Fig. 7. Simulated open-circuit voltage  $V_{OC}$  versus incident light intensity with different surface recombination velocities  $S_p$  (unit:  $\text{m s}^{-1}$ ) for holes at anode. The same injection barrier of 0.4 eV between the anode and active layer is assumed.

results of Fig. 3b and c. The experimental  $J$ - $V$  characteristics of pristine GO and  $\text{MoO}_x$  cases show noticeable curve bending at the forward bias regime, compared to the cases with GO:F5BnPA and  $\text{MoO}_x$ :F5BnPA. The large mismatch between HOMO of SMPV1 and GO WF induces a large HIB at the anode and thus a low  $V_{OC}$ . After introducing the F5BnPA into the GO, the reduced barrier contributes to the largely improved  $V_{OC}$  and S-shape  $J$ - $V$  curve elimination.

The relation between  $V_{OC}$  and  $I$  under different injection barrier and surface recombination velocity conditions at the anode is also studied. When an infinite surface recombination velocity of holes (majority carriers at the anode) is assumed (and unchanged), the slope of the curve ( $V_{OC} \sim \log(I)$ ) is independent of the values of injection barriers, as shown in Fig. 6, which cannot explain the phenomenon observed in Fig. 4. However, when the surface recombination velocity decreases (with the same injection barrier settings), we clearly see a reduced slope depicted in Fig. 7. This interesting finding is well coincident with the experimental results illustrated in Fig. 4. From the above theoretical analysis and the experimental results in previous section, the introduction of F5BnPA not only reduces the (equivalent) injection barrier but also increases the surface recombination velocity between GO or  $\text{MoO}_x$  anode and active layers. As a consequence, hole collection are remarkably improved by the incorporation of F5BnPA in HTLs. The eliminated S-shaped  $J$ - $V$  characteristics (Fig. 3b), enhanced  $V_{OC}$  (Fig. 3b, c), and increased slope of  $V_{OC} \sim \log(I)$  curve (Fig. 4) are experimentally and theoretically verified and explained for the improved electrical properties of OSCs by the incorporation of F5BnPA in HTLs.

## Experimental Section

### Preparation of GO:F5BnPA and $\text{MoO}_x$ :F5BnPA blend films

Molybdenum powder was purchased from Aladdin Industrial Inc. F5BnPA was purchased from Sigma-Aldrich. PEDOT:PSS

(Baytron Al 4083) was purchased from H. C. Starck GmbH, Germany. Graphene oxide was synthesized by a reported modified Hummer's method<sup>67</sup> and was dispersed into ethanol under ultrasonication to form a 0.2 mg mL<sup>-1</sup> solution. Molybdenum bronze solution was prepared by a former reported method.<sup>26, 28</sup> Different amounts of F5BnPA were added into the two solutions to form blend solutions with certain concentrations, respectively. Different hole transport layers were prepared by spin-coating the mixed solutions onto clean ITO substrates at 4000 rpm for 40 s.

### Devices Fabrication

ITO glasses were cleaned by a standard procedure with detergent, acetone, and ethanol ultrasonic bath for each of 10 min, followed by an ultraviolet-ozone (UVO) treatment of 15 min. PEDOT:PSS was spin-coated on the treated ITO at 4000 rpm for 40s and followed by 120 °C annealing for 20 min. The active layer was deposited by spin-coating the blend solution of SMPV1:PC<sub>71</sub>BM with a weight ratio of 1:0.8 onto ITO/HTL substrates in glove box at 2000 rpm. The blend solution was prepared in solvent of chloroform. For the OSCs, Calcium (20 nm) and aluminum (100 nm) were thermally evaporated onto the active layer through the same shadow mask under the pressure of 10<sup>-6</sup> Torr. For the hole only devices, MoOx (10 nm) and silver (100 nm) were thermally evaporated.

### Measurement and Characterization

The *J-V* characterizations of the OSCs were carried out under a light intensity of 100 mW cm<sup>-2</sup> or dark by using a Keithley 2635 source meter with a step length of 0.01 V. The light was produced by ABET AM 1.5 G solar simulator and its intensity was calibrated by a monocrystalline silicon standard solar cell. The more accurate *V*<sub>OC</sub> values under different light intensity were obtained by *J-V* characterization around the open circuit state with a step length of 0.001 V. The WF of different hole transporting layers were measured by SKP 5050 Scanning Kelvin-Probe System (KP Technology Ltd.) with a resolution of 1-3 meV. UPS was conducted using a He I discharged lamp (21.22 eV, Kratos Analytical). Height images and surface potential images were measured by tapping-mode AFM (NT-MDT, Moscow, Russia). The thickness of different HTLs were characterized by spectroscopic ellipsometer (J.A. WOOLLAM CO. INC.).

### Theoretical model

The electrical properties of OSCs can be modeled by solving organic semiconductor equations involving Poisson, drift-diffusion and continuity equations<sup>68, 69</sup>

$$\nabla \cdot (\varepsilon \nabla \phi) = -q(p - n) \quad (1)$$

$$\frac{\partial n}{\partial t} = \frac{1}{q} \nabla \cdot (-q\mu_n n \nabla \phi + qD_n \nabla n) + QG - (1-Q)R \quad (2)$$

$$\frac{\partial p}{\partial t} = -\frac{1}{q} \nabla \cdot (-q\mu_p p \nabla \phi - qD_p \nabla p) + QG - (1-Q)R \quad (3)$$

where *q* is the electron charge,  $\phi$  is the potential, and *n* and *p* are electron and hole densities, respectively. Moreover,  $\mu_n$  and  $\mu_p$  are the mobility of electrons and holes respectively. Furthermore, and  $D_n = \mu_n(k_B T/q)$  are  $D_p = \mu_p(k_B T/q)$  the diffusion coefficients of electrons and holes respectively, where  $k_B$  and *T* are Boltzmann constant and kelvin temperature.  $J_n = -q\mu_n n \nabla \phi + qD_n \nabla n$  and  $J_p = -q\mu_p p \nabla \phi - qD_p \nabla p$  are respectively electron and hole current densities, and *G* is the exciton generation rate. Here, the recombination rate *R* is taken as the Langevin bimolecular form<sup>70</sup>; and the field-dependent exciton dissociation probability *Q* is evaluated by the Onsager-Braun theory.<sup>71, 72</sup> The potential boundary condition at the electrodes is given by

$$\phi = V - \frac{W_m}{q} \quad (4)$$

where *V* is the applied bias voltage and *W<sub>m</sub>* is the WF of the electrode. For understanding the influence of electrodes on the electrical properties of OSCs, the current density (boundary conditions) at the Schottky contacts are given by

$$\text{Anode} \begin{cases} J_n^a = qS_n^a(n - n_{eq}^a) \\ J_p^a = qS_p^a(p - p_{eq}^a) \end{cases} \quad \text{Cathode} \begin{cases} J_n^c = qS_n^c(n - n_{eq}^c) \\ J_p^c = qS_p^c(p - p_{eq}^c) \end{cases} \quad (4)$$

where  $S_n^a$  and  $S_p^a$  are the surface recombination velocity for electrons and holes at anode;  $S_n^c$  and  $S_p^c$  are the surface recombination velocity for electrons and holes at cathode.  $n_{eq}$  and  $p_{eq}$  are electron and hole densities with assumptions of surface infinite recombination velocities

$$\text{Anode} \begin{cases} n_{eq}^a = N_c \exp\left(\frac{-E_g + q\phi_p}{k_B T}\right) \\ p_{eq}^a = N_v \exp\left(\frac{-q\phi_p}{k_B T}\right) \end{cases} \quad \text{Cathode} \begin{cases} n_{eq}^c = N_c \exp\left(\frac{-q\phi_n}{k_B T}\right) \\ p_{eq}^c = N_v \exp\left(\frac{-E_g + q\phi_n}{k_B T}\right) \end{cases} \quad (5)$$

where  $N_c$  and  $N_v$  are the effective density of states for bulk heterojunction active materials.  $\phi_n$  and  $\phi_p$  are injection barriers for cathode and anode, respectively. In our simulation,  $S_n^c \rightarrow \infty$ ,  $S_p^c \rightarrow \infty$ ,  $S_n^a \rightarrow \infty$  and  $\phi_n = 0$ . We modify  $\phi_p$  and  $S_p^a$  to clarify the roles of injection barrier and surface recombination velocities of holes (majorities) at the anode in affecting electrical performance of OSCs.

### Conclusions

To sum up, we propose and demonstrate an effective low-temperature and solution-process approach to tune the WF of HTLs for good energy level alignment between electrodes and deep HOMO-level donor materials. Distinctively, this wide WF tuning approach works in two different types of HTL materials represented by GO and MoO<sub>x</sub>, whose carriers transport is via VB and CB respectively. Both Kelvin-Probe measurements and UPS results confirm the continuously tunable WF for GO and MoO<sub>x</sub> HTLs is achieved after a simple F5BnPA incorporation. Employing a deep HOMO-level donor material of SMPV1, OSCs



## ARTICLE

## Journal of Materials Chemistry A

utilizing F5BnPA:GO and F5BnPA:GO MoO<sub>x</sub> HTLs can achieve improved  $V_{OC}$  and  $J_{SC}$ , then thus greatly enhanced PCE compared with OSCs utilizing pristine GO and MoO<sub>x</sub> HTLs. Our experimental and theoretical results show that the improved performance are attributed to the reduced (equivalent) injection barrier for enhancing  $V_{OC}$  and increased surface recombination velocity for eliminating S-shaped  $J$ - $V$ . Therefore, our approach for introducing F5BnPA into HTLs could effectively improve the electrical properties of deep HOMO-level donor based OSCs. Consequently, the proposed new approach of F5BnPA incorporated GO and MoO<sub>x</sub> HTLs with large WF tuning capacity makes an attractive contribution to the evolution of high  $V_{OC}$  OSCs with deep HOMO-level donors and can also be applied into other organic electronic devices.

### Acknowledgements

J.C. and F.X. contributed equally to the work. This study was supported by the University Grant Council of the University of Hong Kong (Grants10401466 and 201111159062), the General Research Fund (Grants HKU711813), an RGC-NSFC Grant (N\_HKU709/12), the Collaborative Research Fund (grant CUHK1/CRF/12G) from the Research Grants Council of Hong Kong Special Administrative Region, China, and Grant CAS14601 from CAS-Croucher Funding Scheme for Joint Laboratories. We acknowledge the help and discussion of Hugh Zhu, Di Zhang and Shunmian Lu.

### Notes and references

1. Y. Liu, C.-C. Chen, Z. Hong, J. Gao, Y. M. Yang, H. Zhou, L. Dou, G. Li and Y. Yang, *Sci. Rep.*, 2013, **3**, 3356.
2. J. You, L. Dou, K. Yoshimura, T. Kato, K. Ohya, T. Moriarty, K. Emery, C.-C. Chen, J. Gao, G. Li and Y. Yang, *Nat. Commun.*, 2013, **4**, 1446.
3. J.-D. Chen, C. Cui, Y.-Q. Li, L. Zhou, Q.-D. Ou, C. Li, Y. Li and J.-X. Tang, *Adv. Mater.*, 2015, **27**, 1035-1041.
4. X. Che, X. Xiao, J. D. Zimmerman, D. Fan and S. R. Forrest, *Adv. Energy Mater.*, 2014, **4**, 1400568.
5. Z. He, B. Xiao, F. Liu, H. Wu, Y. Yang, S. Xiao, C. Wang, T. P. Russell and Y. Cao, *Nat. Photon.*, 2015, **9**, 174-179.
6. Y. Liu, J. Zhao, Z. Li, C. Mu, W. Ma, H. Hu, K. Jiang, H. Lin, H. Ade and H. Yan, *Nat. Commun.*, 2014, **5**, 5293.
7. B. Kan, Q. Zhang, M. Li, X. Wan, W. Ni, G. Long, Y. Wang, X. Yang, H. Feng and Y. Chen, *J. Am. Chem. Soc.*, 2014, **136**, 15529-15532.
8. G. Yu, J. Gao, J. C. Hummelen, F. Wudl and A. J. Heeger, *Science*, 1995, **270**, 1789-1790.
9. M. C. Scharber, M. Koppe, J. Gao, F. Cordella, M. A. Loi, P. Denk, M. Morana, H.-J. Egelhaaf, K. Forberich, G. Dennler, R. Gaudiana, D. Waller, Z. Zhu, X. Shi and C. J. Brabec, *Adv. Mater.*, 2010, **22**, 367-370.
10. G. Li, V. Shrotriya, J. Huang, Y. Yao, T. Moriarty, K. Emery and Y. Yang, *Nat. Mater.*, 2005, **4**, 864-868.
11. S. Lu, X. Guan, X. Li, W. E. I. Sha, F. Xie, H. Liu, J. Wang, F. Huang and W. C. H. Choy, *Adv. Energy Mater.*, 2015, DOI: 10.1002/aenm.201500631.
12. H. Zhou, Y. Zhang, C.-K. Mai, S. D. Collins, G. C. Bazan, T.-Q. Nguyen and A. J. Heeger, *Adv. Mater.*, 2015, **27**, 1767-1773.
13. T. Yang, M. Wang, C. Duan, X. Hu, L. Huang, J. Peng, F. Huang and X. Gong, *Energy Environ. Sci.*, 2012, **5**, 8208-8214.
14. F. Jiang, W. C. H. Choy, X. Li, D. Zhang and J. Cheng, *Adv. Mater.*, 2015, **27**, 2930-2937.
15. A. Varotto, N. D. Treat, J. Jo, C. G. Shuttle, N. A. Batarra, F. G. Brunetti, J. H. Seo, M. L. Chabynyc, C. J. Hawker, A. J. Heeger and F. Wudl, *Angew. Chem. Int. Edit.*, 2011, **50**, 5166-5169.
16. L. Dou, J. You, Z. Hong, Z. Xu, G. Li, R. A. Street and Y. Yang, *Adv. Mater.*, 2013, **25**, 6642-6671.
17. X. Gong, M. Tong, F. G. Brunetti, J. Seo, Y. Sun, D. Moses, F. Wudl and A. J. Heeger, *Adv. Mater.*, 2011, **23**, 2272-2277.
18. P. W. Blom, V. D. Mihailetchi, L. J. A. Koster and D. E. Markov, *Adv. Mater.*, 2007, **19**, 1551-1566.
19. W. Tress, K. Leo and M. Riede, *Adv. Funct. Mater.*, 2011, **21**, 2140-2149.
20. J. Reinhardt, M. Grein, C. Bühler, M. Schubert and U. Würfel, *Adv. Energy Mater.*, 2014, **4**, 1400081.
21. E. L. Ratcliff, A. Garcia, S. A. Paniagua, S. R. Cowan, A. J. Giordano, D. S. Ginley, S. R. Marder, J. J. Berry and D. C. Olson, *Adv. Energy Mater.*, 2013, **3**, 647-656.
22. C.-Z. Li, C.-Y. Chang, Y. Zang, H.-X. Ju, C.-C. Chueh, P.-W. Liang, N. Cho, D. S. Ginger and A. K. Y. Jen, *Adv. Mater.*, 2014, **26**, 6262-6267.
23. A. Wagenpfahl, D. Rauh, M. Binder, C. Deibel and V. Dyakonov, *Phys. Rev. B*, 2010, **82**, 115306.
24. M. Jørgensen, K. Norrman and F. C. Krebs, *Sol. Energy Mater. Sol. Cells*, 2008, **92**, 686-714.
25. J. Meyer, S. Hamwi, M. Kröger, W. Kowalsky, T. Riedl and A. Kahn, *Adv. Mater.*, 2012, **24**, 5408-5427.
26. X. Li, W. C. H. Choy, F. Xie, S. Zhang and J. Hou, *J. Mater. Chem. A*, 2013, **1**, 6614-6621.
27. V. Shrotriya, G. Li, Y. Yao, C.-W. Chu and Y. Yang, *Appl. Phys. Lett.*, 2006, **88**, 073508.
28. F. Xie, W. C. H. Choy, C. Wang, X. Li, S. Zhang and J. Hou, *Adv. Mater.*, 2013, **25**, 2051-2055.
29. S. Han, W. S. Shin, M. Seo, D. Gupta, S.-J. Moon and S. Yoo, *Org. Electron.*, 2009, **10**, 791-797.
30. S.-S. Li, K.-H. Tu, C.-C. Lin, C.-W. Chen and M. Chhowalla, *ACS Nano*, 2010, **4**, 3169-3174.
31. Y. Gao, H.-L. Yip, S. K. Hau, K. M. O'Malley, N. C. Cho, H. Chen and A. K.-Y. Jen, *Appl. Phys. Lett.*, 2010, **97**, 203306.
32. D. Yang, L. Zhou, W. Yu, J. Zhang and C. Li, *Adv. Energy Mater.*, 2014, **4**, 1400591.
33. M. D. Irwin, D. B. Buchholz, A. W. Hains, R. P. H. Chang and T. J. Marks, *PNAS*, 2008, **105**, 2783-2787.
34. K. X. Steirer, J. P. Chesin, N. E. Widjonarko, J. J. Berry, A. Miedaner, D. S. Ginley and D. C. Olson, *Org. Electron.*, 2010, **11**, 1414-1418.
35. S. Chen, J. R. Manders, S.-W. Tsang and F. So, *J. Mater. Chem.*, 2012, **22**, 24202-24212.
36. D. Yang, L. Zhou, L. Chen, B. Zhao, J. Zhang and C. Li, *Chem. Commun.*, 2012, **48**, 8078-8080.
37. J. Liu, Y. Xue and L. Dai, *J. Phys. Chem. Lett.*, 2012, **3**, 1928-1933.
38. E. Stratakis, K. Savva, D. Konios, C. Petridis and E. Kymakis, *Nanoscale*, 2014, **6**, 6925-6931.

39. C. Li, X. Yang, Y. Zhao, P. Zhang, Y. Tu and Y. Li, *Org. Electron.*, 2014, **15**, 2868-2875.
40. J. Liu, Y. H. Xue, Y. X. Gao, D. S. Yu, M. Durstock and L. M. Dai, *Adv. Mater.*, 2012, **24**, 2228-2233.
41. G. Kakavelakis, D. Konios, E. Stratakis and E. Kymakis, *Chem. Mater.*, 2014, **26**, 5988-5993.
42. J. Liu, M. Durstock and L. Dai, *Energy Environ. Sci.*, 2014, **7**, 1297-1306.
43. A. Sharma, A. Haldi, W. J. Potscavage Jr, P. J. Hotchkiss, S. R. Marder and B. Kippelen, *J. Mater. Chem.*, 2009, **19**, 5298-5302.
44. P. J. Hotchkiss, H. Li, P. B. Paramonov, S. A. Paniagua, S. C. Jones, N. R. Armstrong, J.-L. Brédas and S. R. Marder, *Adv. Mater.*, 2009, **21**, 4496-4501.
45. N. Kedem, S. Blumstengel, F. Henneberger, H. Cohen, G. Hodes and D. Cahen, *Phys. Chem. Chem. Phys.*, 2014, **16**, 8310-8319.
46. I. Lange, S. Reiter, M. Pätzelt, A. Zykov, A. Nefedov, J. Hildebrandt, S. Hecht, S. Kowarik, C. Wöll, G. Heimel and D. Neher, *Adv. Funct. Mater.*, 2014, **24**, 7014-7024.
47. I. Lange, S. Reiter, J. Kniepert, F. Piersimoni, M. Pätzelt, J. Hildebrandt, T. Brenner, S. Hecht and D. Neher, *Appl. Phys. Lett.*, 2015, **106**, 113302.
48. A. Bulusu, S. A. Paniagua, B. A. MacLeod, A. K. Sigdel, J. J. Berry, D. C. Olson, S. R. Marder and S. Graham, *Langmuir*, 2013, **29**, 3935-3942.
49. P. J. Hotchkiss, S. C. Jones, S. A. Paniagua, A. Sharma, B. Kippelen, N. R. Armstrong and S. R. Marder, *Acc. Chem. Res.*, 2011, **45**, 337-346.
50. A. M. Bradley, E. H. Noah, L. R. Erin, L. J. Judith, R. A. Neal, J. G. Anthony, J. H. Peter, R. M. Seth, T. C. Charles and S. G. David, *J. Phys. Chem. Lett.*, 2012, **3**, 1202-1207.
51. K. M. Knesting, H. Ju, C. W. Schlenker, A. J. Giordano, A. Garcia, O. N. L. Smith, D. C. Olson, S. R. Marder and D. S. Ginger, *J. Phys. Chem. Lett.*, 2013, **4**, 4038-4044.
52. H. Wang, E. D. Gomez, Z. Guan, C. Jaye, M. F. Toney, D. A. Fischer, A. Kahn and Y.-L. Loo, *J. Phys. Chem. C*, 2013, **117**, 20474-20484.
53. G. Shao, M. S. Glaz, F. Ma, H. Ju and D. S. Ginger, *ACS Nano*, 2014, **8**, 10799-10807.
54. R. C. Sarah, V. L. Jian, C. O. Dana and L. R. Erin, *Adv. Energy Mater.*, 2014, **5**, 1400549.
55. D. J. Ellison, B. Lee, V. Podzorov and C. D. Frisbie, *Adv. Mater.*, 2011, **23**, 502-507.
56. A. Van Hengstum, J. Van Ommen, H. Bosch and P. Gellings, *Appl. Catal.*, 1983, **5**, 207-217.
57. A. M. Turek, I. E. Wachs and E. DeCanio, *J. Phys. Chem.*, 1992, **96**, 5000-5007.
58. M. Zhang, H. Wang, H. Tian, Y. Geng and C. W. Tang, *Adv. Mater.*, 2011, **23**, 4960-4964.
59. L. Huo, J. Hou, S. Zhang, H.-Y. Chen and Y. Yang, *Angew. Chem. Int. Edit.*, 2010, **49**, 1500-1503.
60. J. Sun, Y. Zhu, X. Xu, L. Lan, L. Zhang, P. Cai, J. Chen, J. Peng and Y. Cao, *J. Phys. Chem. C*, 2012, **116**, 14188-14198.
61. O. J. Sandberg, M. Nyman and R. Österbacka, *Phys. Rev. Applied*, 2014, **1**, 024003.
62. D. Zhang, W. C. H. Choy, F. Xie, W. E. I. Sha, X. Li, B. Ding, K. Zhang, F. Huang and Y. Cao, *Adv. Funct. Mater.*, 2013, **23**, 4255-4261.
63. A. M. Goodman and A. Rose, *J. Appl. Phys.*, 1971, **42**, 2823-2830.
64. M. M. Mandoc, F. B. Kooistra, J. C. Hummelen, B. de Boer and P. W. M. Blom, *Appl. Phys. Lett.*, 2007, **91**, 263505.
65. V. D. Mihailetchi, H. Xie, B. de Boer, L. J. A. Koster and P. W. Blom, *Adv. Funct. Mater.*, 2006, **16**, 699-708.
66. L. J. A. Koster, V. D. Mihailetchi, R. Ramaker and P. W. M. Blom, *Appl. Phys. Lett.*, 2005, **86**, 123509.
67. M. Hirata, T. Gotou, S. Horiuchi, M. Fujiwara and M. Ohba, *Carbon*, 2004, **42**, 2929-2937.
68. S. Selberherr, *Analysis and simulation of semiconductor devices*, Springer, 1st edn., 1984.
69. L. J. A. Koster, E. C. P. Smits, V. D. Mihailetchi and P. W. M. Blom, *Phys. Rev. B*, 2005, **72**, 085205.
70. P. Langevin, *Ann. Chim. Phys*, 1903, **28**, 122.
71. L. Onsager, *Phys. Rev.*, 1938, **54**, 554.
72. C. L. Braun, *J. Chem. Phys.*, 1984, **80**, 4157-4161.

**Table of Contents (Toc)**

An efficient and wide work function tuning approach of hole transport layers for deep HOMO level organic solar cells.

